

Crystal structure of diroximel fumarate, $C_{11}H_{13}NO_6$ James A. Kaduk^{1,2} , Anja Dosen³  and Thomas N. Blanton³ ¹Illinois Institute of Technology, Chicago IL 60616²North Central College, Naperville, IL 60540, USA³ICDD, Newtown Square, PA, 19073-3273, USA

(Received 24 October 2024; revised 11 January 2025; accepted 14 January 2025)

Abstract: The crystal structure of diroximel fumarate has been solved and refined using synchrotron X-ray powder diffraction data, and optimized using density functional theory techniques. Diroximel fumarate crystallizes in space group $P-1$ (#2) with $a = 6.12496(15)$, $b = 8.16516(18)$, $c = 12.7375(6)$ Å, $\alpha = 85.8174(21)$, $\beta = 81.1434(12)$, $\gamma = 71.1303(3)^\circ$, $V = 595.414(23)$ Å³, and $Z = 2$ at 298 K. The crystal structure consists of interleaved double layers of hook-shaped molecules parallel to the ab -plane. The side chains form the inner portion of the layers, and the rings comprise the outer surfaces. There are no classical hydrogen bonds in the structure, but 9 C–H...O hydrogen bonds contribute to the crystal energy. The powder pattern has been submitted to ICDD for inclusion in the Powder Diffraction File™ (PDF®).

© The Author(s), 2025. Published by Cambridge University Press on behalf of International Center for Diffraction Data. This is an Open Access article, distributed under the terms of the Creative Commons Attribution licence (<http://creativecommons.org/licenses/by/4.0>), which permits unrestricted re-use, distribution and reproduction, provided the original article is properly cited. [doi:10.1017/S0885715625000119]

Key words: crystal structure, diroximel fumarate, density functional theory, rietveld refinement, Vumerity®

I. INTRODUCTION

Diroximel fumarate, $C_{11}H_{13}NO_6$, (marketed under the trade name Vumerity) is used for treating multiple sclerosis, acting as an anti-inflammatory and immunosuppressant. As a formulary, Vumerity is administered as a capsule, dissolving in the intestine. The systematic name (CAS Registry Number 1577222-14-0) is 4-O-[2-(2,5-dioxopyrrolidin-1-yl)ethyl] 1-O-methyl (E)-but-2-enedioate. A two-dimensional molecular diagram of diroximel fumarate is shown in Figure 1.

Powder patterns for crystalline diroximel fumarate and amorphous solid dispersions are reported in International Patent Application WO 2021/053476 A1 (Chand et al., 2021; Glenmark Life Sciences Ltd.). This work was carried out as part of a project (Kaduk et al., 2014) to determine the crystal structures of large-volume commercial pharmaceuticals, and include high-quality powder diffraction data for them in the Powder Diffraction File (Kabekkodu et al., 2024).

II. EXPERIMENTAL

Diroximel fumarate was a commercial reagent, purchased from TargetMol (Batch # 117380), and was used as received. The white powder was packed into a 0.5 mm diameter Kapton capillary and rotated during the measurement at ~2 Hz. The powder pattern was measured at 298(1) K at the Wiggler Low Energy Beamline (Leontowich et al., 2021) of the Brookhouse

X-ray Diffraction and Scattering Sector of the Canadian Light Source using a wavelength of 0.819563(2) Å (15.1 keV) from 1.6 to 75.0° 2θ with a step size of 0.0025° and a collection time of 3 min. The high-resolution powder diffraction data were collected using eight Dectris Mythen2 X series 1 K linear strip detectors. NIST SRM 660b LaB₆ was used to calibrate the instrument and refine the monochromatic wavelength used in the experiment.

The peaks were located by interactive profile fitting using JADE Pro (MDI, 2024), and the pattern was indexed (permitting up to 3 unindexed lines) with DICVOL14 (Louër and Boulif, 2014) on a primitive triclinic unit cell ($M(20) = 66.5$, $F(20) = 253.0$) with $a = 6.1213(15)$, $b = 8.1557(17)$, $c = 12.7303(17)$ Å, $\alpha = 85.839(20)$, $\beta = 81.146(20)$,

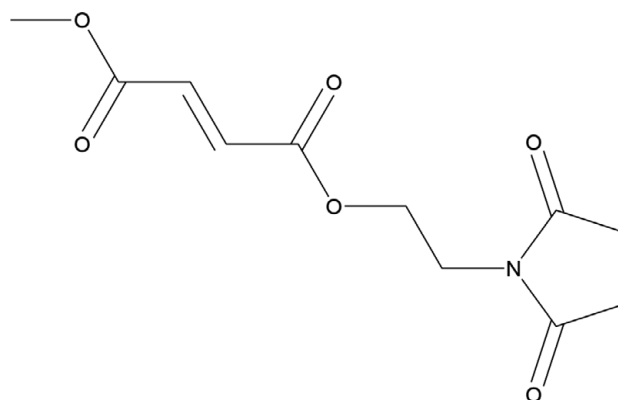


Figure 1. The two-dimensional structure of diroximel fumarate.

Corresponding author: James A. Kaduk; Email: kaduk@polycrystallography.com



$\gamma = 71.136(20)^\circ$, $V = 594.09 \text{ \AA}^3$, and $Z = 2$. The space group was assumed to be $P-1$, which was confirmed by the successful solution and refinement of the structure. A reduced cell search of the Cambridge Structural Database (Groom *et al.*, 2016) yielded no hits.

The diroximel fumarate molecule was downloaded from PubChem (Kim *et al.*, 2023) as Conformer3D_COMPOUND_CID_73330464.sdf. It was converted to a *.mol2 file using Mercury (Macrae *et al.*, 2020). The crystal structure was solved using Monte Carlo simulated annealing techniques as implemented in EXPO2014 (Altomare *et al.*, 2013). Eight of the 10 trials yielded essentially the same solution.

Rietveld refinement was carried out with GSAS-II (Toby and Von Dreele, 2013). Only the $3.5\text{--}50.0^\circ$ portion of the pattern was included in the refinements ($d_{\min} = 0.969 \text{ \AA}$). All non-H bond distances and angles were subjected to restraints, based on a Mercury/Mogul Geometry Check (Sykes *et al.*, 2011, Bruno *et al.*, 2004). The Mogul average and standard deviation for each quantity were used as the restraint parameters. The dioxopyrrolidine rings were restrained to be planar. The restraints contributed 2.7% to the overall χ^2 . The hydrogen atoms were included in calculated positions, which were recalculated during the refinement using Materials Studio (Dassault Systèmes, 2023). The U_{iso} of the heavy atoms were grouped by chemical similarity. The U_{iso} for the H atoms was fixed at $1.3\times$ the U_{iso} of the heavy atoms to which they are attached. The peak profiles were described using the generalized microstrain model (Stephens, 1999). Preferred orientation was described using a second-order spherical harmonics model (Von Dreele, 1997). The background was modeled using a 6-term shifted Chebyshev polynomial, with a peak at 10.86° to model the scattering from the Kapton capillary and any amorphous component.

The final refinement of 94 variables using 18,601 observations and 42 restraints yielded the residual $R_{\text{wp}} = 0.0424$. The largest peak (1.51 \AA from C8) and hole (0.90 \AA from C18)

in the difference Fourier map were $0.55(11)$ and $-0.41(11) e\text{\AA}^{-3}$, respectively. The final Rietveld plot is shown in Figure 2. The largest features in the normalized error plot are in the description of the amorphous scattering and the shapes and positions of some of the low-angle peaks. These misfits probably indicate a change in the specimen during the measurement.

The crystal structure of diroximel fumarate was optimized (fixed experimental unit cell) with density functional theory techniques using VASP (Kresse and Furthmüller, 1996) through the MedeA graphical interface (Materials Design, 2024). The calculation was carried out on 32 cores of a 144-core (768 Gb memory) HPE Superdome Flex 280 Linux server at North Central College. The calculation used the GGA-PBE functional, a plane wave cutoff energy of 400.0 eV, and a k -point spacing of 0.5 \AA^{-1} leading to a $3 \times 2 \times 1$ mesh, and took ~ 23 min. Single-point density functional theory calculations (fixed experimental cell) and population analysis were carried out using CRYSTAL23 (Erba *et al.*, 2023) and CRYSTAL17 (Dovesi *et al.*, 2018). The basis sets for the H, C, N, and O atoms in the calculation were those of Gatti *et al.* (1994). The calculations were run on a 3.5 GHz PC using 8 k -points and the B3LYP functional and took ~ 1.0 h.

III. RESULTS AND DISCUSSION

This synchrotron pattern of diroximel fumarate matches that of Chand *et al.* (2021) well enough to conclude that they represent the same material, and thus that our material is representative (Figure 3). The root-mean-square Cartesian displacement of the non-H atoms in the Rietveld-refined and VASP-optimized molecules is 0.076 \AA (Figure 4). The agreement is within the normal range for correct structures (van de Streek and Neumann, 2014). The major difference is in the orientation of the hydrogen atoms in the methyl group,

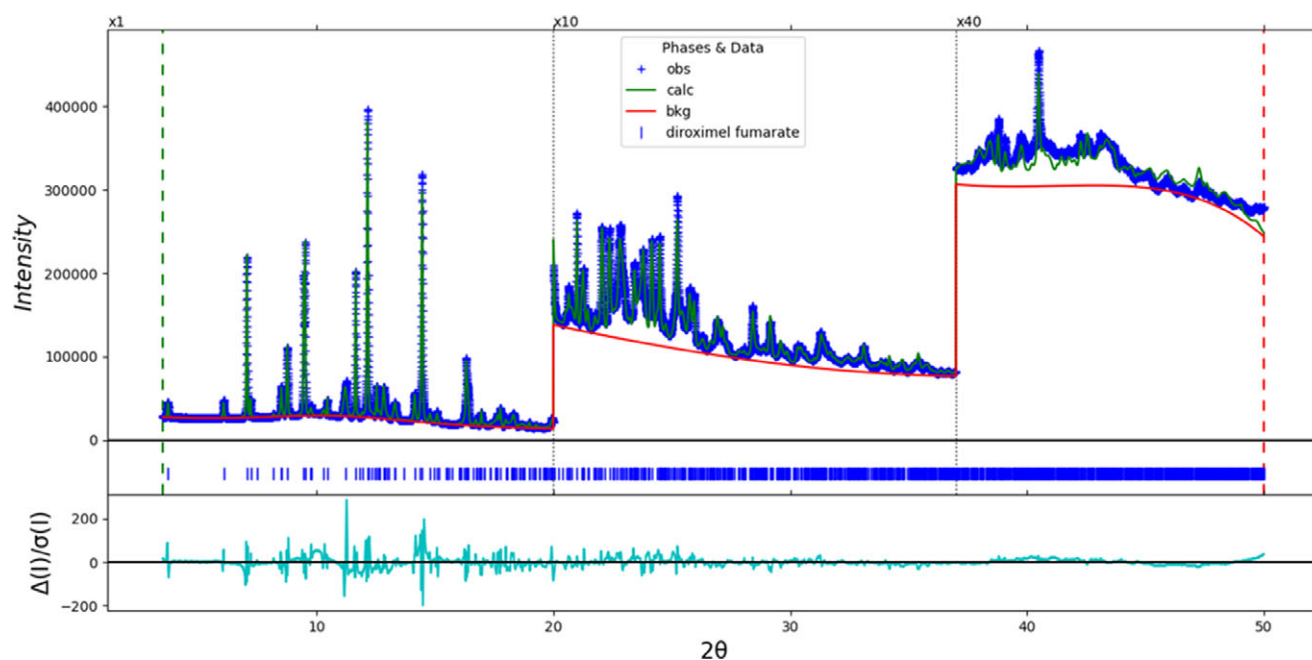


Figure 2. The Rietveld plot for diroximel fumarate. The blue crosses represent the observed data points, and the green line is the calculated pattern. The cyan curve is the normalized error plot, and the red line is the background curve. The vertical scale has been multiplied by a factor of $10\times$ for $2\theta > 20.0^\circ$, and by a factor of $40\times$ for $2\theta > 37.0^\circ$.

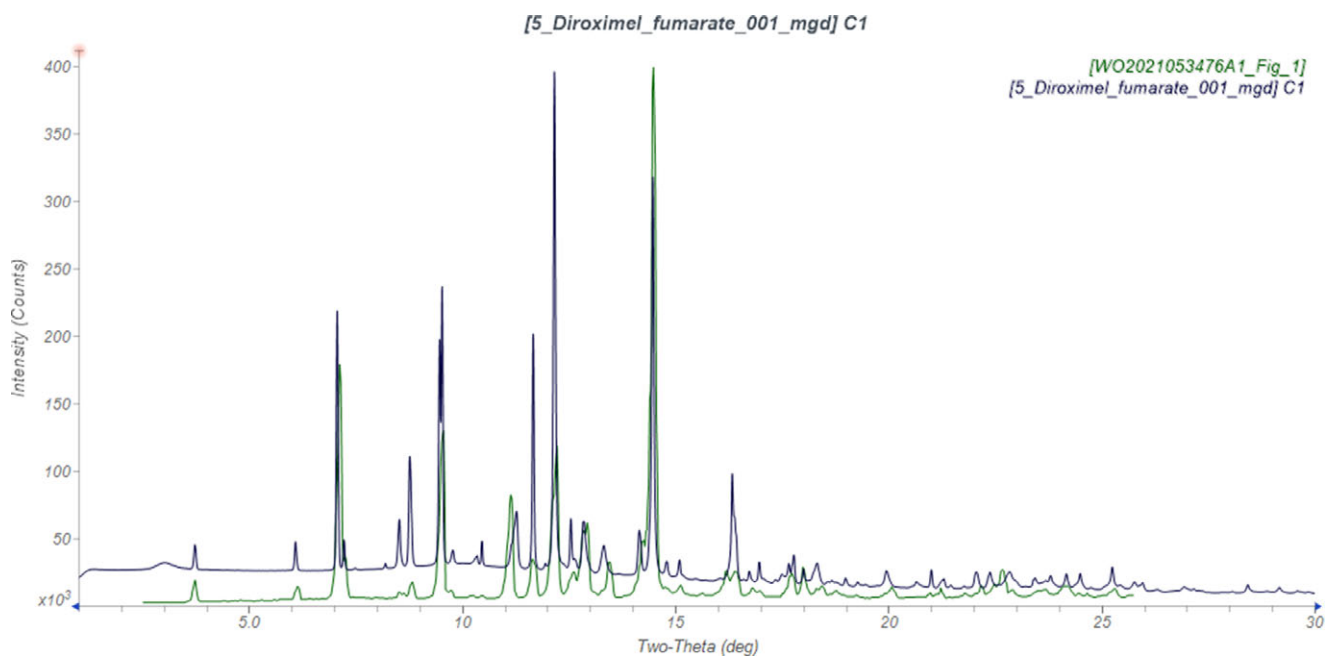


Figure 3. Comparison of the synchrotron pattern of diroxime fumarate (black) to that reported by Chand et al. (2021; green). The literature pattern (measured using Cu K_{α} radiation) was digitized using UN-SCAN-IT (Silk Scientific, 2013) and converted to the synchrotron wavelength of 0.819563(2) Å using JADE Pro (MDI, 2024). Image generated using JADE Pro (MDI, 2024).

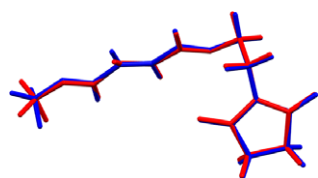


Figure 4. Comparison of the Rietveld-refined (red) and VASP-optimized (blue) structures of diroxime fumarate. The root-mean-square Cartesian displacement is 0.076 Å. Image generated using Mercury (Macrae et al., 2020).

but this is to be expected since those positions were calculated using force field techniques. The asymmetric unit is illustrated in Figure 5. The remaining discussion will emphasize the VASP-optimized structure.

All bond distances, bond angles, and torsion angles fall within the normal ranges indicated by a Mercury Mogul

Geometry check (Macrae et al., 2020). Quantum chemical geometry optimization of the isolated molecule (DFT/B3LYP/6-31G*/water) using Spartan '24 (Wavefunction, 2023) indicated that the observed conformation is 1.8 kcal/mol lower in energy than the local minimum, which has a similar conformation (rms displacement = 0.306 Å). The global minimum-energy conformation is 6.6 kcal/mol lower in energy, but has a kinked side chain, showing that intermolecular interactions are important in determining the solid-state conformation.

The crystal structure (Figure 6) consists of interleaved double layers of hook-shaped molecules parallel to the *ab*-plane. The side chains form the inner portion of the layers, and the rings comprise the outer surfaces. The mean plane of the side chain is approximately 0, 9, -8, and that of the dioxopyrrolidine ring is -7, -14, 25.

Analysis of the contributions to the total crystal energy of the structure using the Forcite module of Materials Studio

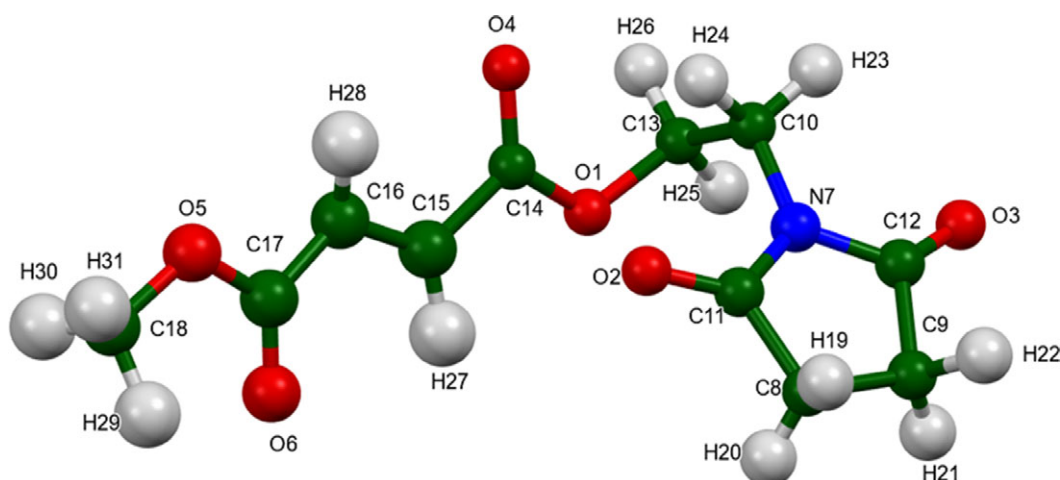


Figure 5. The asymmetric unit of diroxime fumarate, with the atom numbering. The atoms are represented by 50% probability spheroids. Image generated using Mercury (Macrae et al., 2020).

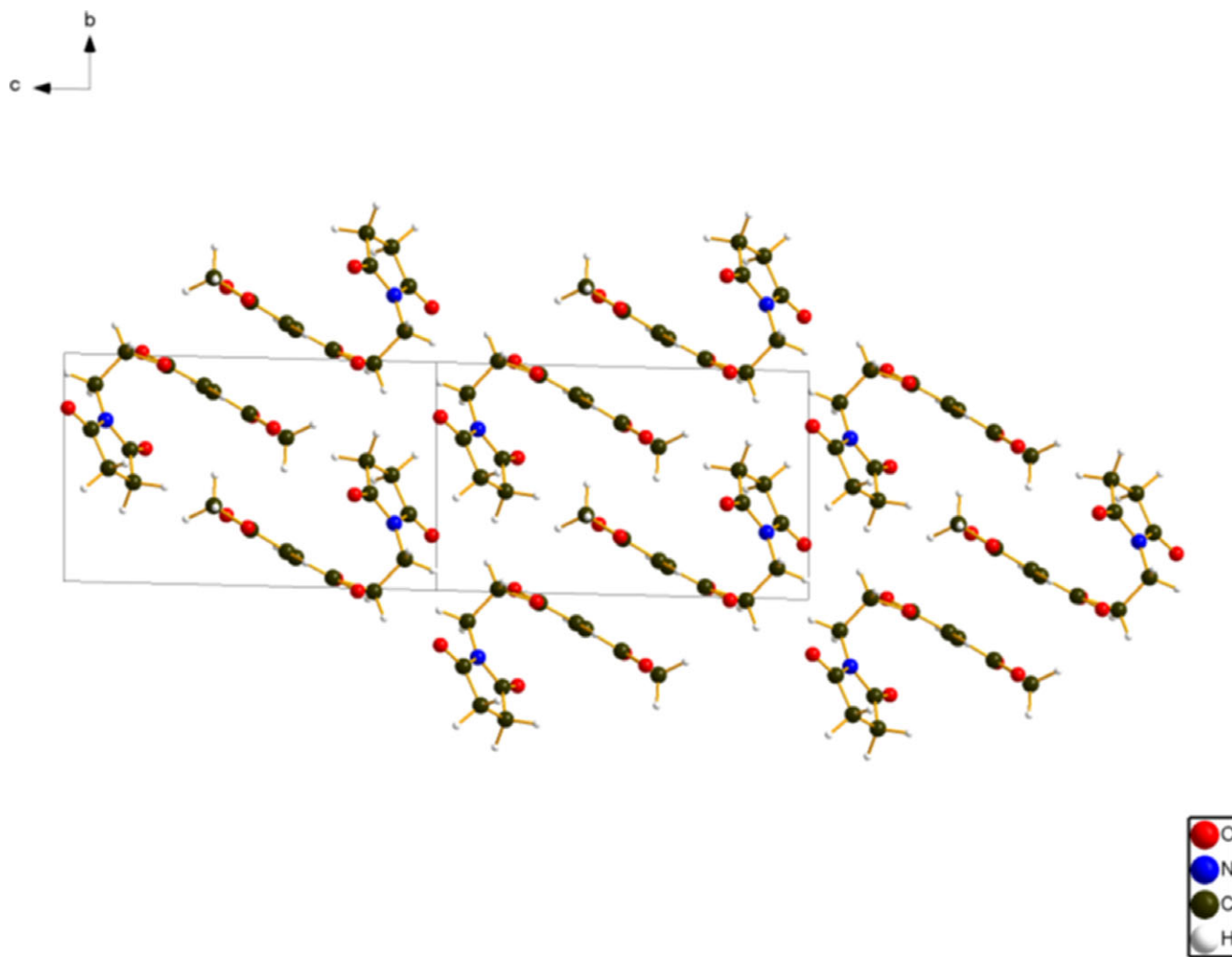


Figure 6. The crystal structure of diroximel fumarate, is viewed down the a -axis. Image generated using Diamond (Crystal Impact, 2023).

(Dassault Systèmes, 2023) indicates that angle distortion terms dominate the intramolecular energy. The intermolecular energy is dominated by electrostatic repulsions. The hydrogen bonds are better discussed using the results of the DFT calculation. There are no classical hydrogen bonds in the structure, but nine C–H...O hydrogen bonds (Table I) contribute to the crystal energy.

The volume enclosed by the Hirshfeld surface of diroximel fumarate (Figure 7, Hirshfeld, 1977, Spackman et al., 2021) is 291.68 \AA^3 , 97.97% of the unit cell volume. The packing density is thus fairly typical. The only significant close contacts (red in Figure 7) involve the hydrogen bonds.

The volume/non-hydrogen atom is smaller than normal, at 16.5 \AA^3 .

The Bravais–Friedel–Donnay–Harker (Bravais, 1866, Friedel, 1907, Donnay and Harker, 1937) algorithm suggests that we might expect platy morphology for diroximel fumarate, with {001} as the major faces. A second-order spherical harmonic model was included in the refinement. The texture index was 1.011(0), indicating that the preferred orientation was not significant in this rotated capillary specimen. The relative intensities in the pattern of Chand et al. (2021) are very different. A refinement using the digitized patent pattern indicates that the specimen was highly textured, with a texture

TABLE I. Hydrogen bonds (CRYSTAL23) in diroximel fumarate.

H-Bond	D–H, Å	H three raised dots, like in the next two columns A, Å	D...A, Å	D–H...A, °	Overlap, e
C18–H31...O6	1.094	2.457	3.547	174.0	0.017
C16–H28...O1	1.091	2.567	3.631	164.7	0.015
C15–H27...O5	1.091	2.593	3.655	164.2	0.015
C13–H25...O4	1.096	2.455	3.512	161.4	0.017
C10–H24...O3	1.099	2.615	3.705	170.9	0.013
C10–H23...O3	1.100	2.495	3.345	121.1	0.010
C9–H22...O3	1.100	2.425	3.360	141.9	0.016
C9–H21...O2	1.100	2.062	3.140	165.9	0.030
C8–H20...O6	1.100	2.402	3.473	164.0	0.018

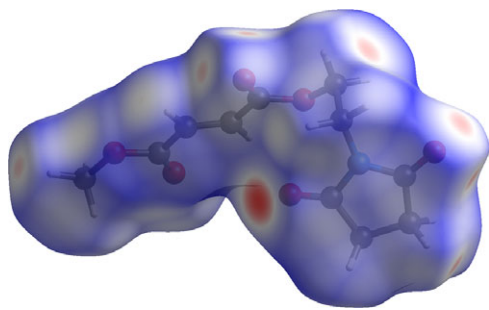


Figure 7. The Hirshfeld surface of diroximel fumarate. Intermolecular contacts longer than the sums of the van der Waals radii are colored blue, and contacts shorter than the sums of the radii are colored red. Contacts equal to the sums of radii are white. Image generated using CrystalExplorer (Spackman et al., 2021).

index >5. We might then expect a significantly preferred orientation in typical flat plate samples of diroximel.

DEPOSITED DATA

The powder pattern of diroximel fumarate from this synchrotron data set has been submitted to ICDD for inclusion in the Powder Diffraction File. The Crystallographic Information Framework (CIF) files containing the results of the Rietveld refinement (including the raw data) and the DFT geometry optimization were deposited with the ICDD. The data can be requested at pdj@icdd.com.

ACKNOWLEDGMENTS

Part of the research described in this article was performed at the Canadian Light Source, a national research facility of the University of Saskatchewan, which is supported by the Canada Foundation for Innovation (CFI), the Natural Sciences and Engineering Research Council (NSERC), the Canadian Institute of Health Research (CIHR), the Government of Saskatchewan, and the University of Saskatchewan. This work was partially supported by the International Centre for Diffraction Data. We thank Adam Leontowich for his assistance in the data collection. We also thank the ICDD team – Megan Rost, Steve Trimble, and Dave Bohnenberger – for their contribution to research, sample preparation, and in-house XRD data collection and verification.

CONFLICTS OF INTEREST

The authors have no conflicts of interest to declare.

REFERENCES

- Altomare, A., C. Cuocci, C. Giacovazzo, A. Moliterni, R. Rizzi, N. Corriero, and A. Falcicchio. 2013. "EXPO2013: A Kit of Tools for Phasing Crystal Structures from Powder Data." *Journal of Applied Crystallography* 46: 1231–1235.
- Bravais, A. 1866. *Etudes Cristallographiques*. Paris, Gauthier Villars.
- Bruno, I. J., J. C. Cole, M. Kessler, J. Luo, W. D. S. Motherwell, L. H. Purkis, B. R. Smith, R. Taylor, R. I. Cooper, S. E. Harris, and A. G. Orpen. 2004. "Retrieval of Crystallographically-Derived Molecular Geometry Information." *Journal of Chemical Information and Computer Sciences* 44: 2133–2144.

- Chand, P., D. V. Patil, S. A. Deshmukh, S. V. Gampawar, V. G. Godase, S. Naik, S. M. Kadam, V. Peddy, V. K. Bhujade, and S. B. Bhirud. 2021. "Process for Preparation of Diroximel Fumarate." International Patent Application WO 2021/053476A1.
- Crystal Impact. 2023. *Diamond V. 5.0.0*. Bonn, Germany. Crystal Impact H. Putz & K. Brandenburg.
- Dassault Systèmes. 2023. *BIOVIA Materials Studio 2024*. San Diego, CA. BIOVIA.
- Donnay, J. D. H., and D. Harker. 1937. "A New Law of Crystal Morphology Extending the Law of Bravais." *American Mineralogist* 22: 446–447.
- Erba, A., J. K. Desmarais, S. Casassa, B. Civalleri, L. Donà, I. J. Bush, B. Searle, L. Maschio, L.-E. Daga, A. Cossard, C. Ribaldone, E. Ascrizzi, N. L. Marana, J.-P. Flament, and B. Kirtman. 2023. "CRYSTAL23: A Program for Computational Solid State Physics and Chemistry." *Journal of Chemical Theory and Computation* 19: 6891–6932; <https://doi.org/10.1021/acs.jctc.2c00958>.
- Friedel, G. 1907. "Etudes sur la loi de Bravais." *Bulletin de la Société Française de Minéralogie* 30: 326–455.
- Gatti, C., V. R. Saunders, and C. Roetti. 1994. "Crystal-Field Effects on the Topological Properties of the Electron-Density in Molecular Crystals – the Case of Urea." *Journal of Chemical Physics* 101: 10686–10696.
- Groom, C. R., I. J. Bruno, M. P. Lightfoot, and S. C. Ward. 2016. "The Cambridge Structural Database." *Acta Crystallographica Section B: Structural Science, Crystal Engineering and Materials* 72: 171–179.
- Hirshfeld, F. L. 1977. "Bonded-Atom Fragments for Describing Molecular Charge Densities." *Theoretica Chimica Acta* 44: 129–138.
- Kabekkodu, S., A. Dosen, and T. N. Blanton. 2024. "PDF-5+: A Comprehensive Powder Diffraction File™ for Materials Characterization." *Powder Diffraction* 39: 47–59.
- Kaduk, J. A., C. E. Crowder, K. Zhong, T. G. Fawcett, and M. R. Suchomel. 2014. "Crystal Structure of Atomoxetine Hydrochloride (Strattera), C₁₇H₂₂NOCl." *Powder Diffraction* 29: 269–273.
- Kim, S., J. Chen, T. Cheng, A. Gindulyte, J. He, S. He, Q. Li, B. A. Shoemaker, P. A. Thiessen, B. Yu, L. Zaslavsky, J. Zhang, and E. E. Bolton. 2023. "PubChem 2023 update." *Nucleic Acids Research* 51(D1): D1373–D1380; doi:10.1093/nar/gkac956.
- Kresse, G., and J. Furthmüller. 1996. "Efficiency of Ab-Initio Total Energy Calculations for Metals and Semiconductors Using a Plane-Wave Basis Set." *Computational Materials Science* 6: 15–50.
- Leontowich, A. F. G., A. Gomez, B. Diaz Moreno, D. Muir, D. Spasyuk, G. King, J. W. Reid, C.-Y. Kim, and S. Kycia. 2021. "The Lower Energy Diffraction and Scattering Side-Bounce Beamline for Materials Science at the Canadian Light Source." *Journal of Synchrotron Radiation* 28: 961–969; <https://doi.org/10.1107/S1600577521002496>.
- Louër, D., and A. Boulfif. 2014. "Some Further Considerations in Powder Diffraction Pattern Indexing with the Dichotomy Method." *Powder Diffraction* 29: S7–S12.
- Macrae, C. F., I. Sovago, S. J. Cottrell, P. T. A. Galek, P. McCabe, E. Pidcock, M. Platings, G. P. Shields, J. S. Stevens, M. Towler, and P. A. Wood. 2020. "Mercury 4.0: From Visualization to Design and Prediction." *Journal of Applied Crystallography* 53: 226–235.
- Materials Design. 2024. *MedeA 3.7.2*. San Diego, CA, Materials Design Inc.
- MDI. 2024. *JADE Pro Version 9.0*. Livermore, CA, Materials Data.
- Silk Scientific. 2013. *UN-SCAN-IT 7.0*. Orem, UT, Silk Scientific Corporation.
- Spackman, P. R., M. J. Turner, J. J. McKinnon, S. K. Wolff, D. J. Grimwood, D. Jayatilaka, and M. A. Spackman. 2021. "CrystalExplorer: A Program for Hirshfeld Surface Analysis, Visualization and Quantitative Analysis of Molecular Crystals." *Journal of Applied Crystallography* 54: 1006–1011; <https://doi.org/10.1107/S1600576721002910>; <https://crystalexplorer.net>.
- Stephens, P. W. 1999. "Phenomenological Model of Anisotropic Peak Broadening in Powder Diffraction." *Journal of Applied Crystallography* 32: 281–289.
- Sykes, R. A., P. McCabe, F. H. Allen, G. M. Battle, I. J. Bruno, and P. A. Wood. 2011. "New Software for Statistical Analysis of Cambridge Structural Database Data." *Journal of Applied Crystallography* 44: 882–886.

- Toby, B. H., and R. B. Von Dreele. 2013. "GSAS II: The Genesis of a Modern Open Source All Purpose Crystallography Software Package." *Journal of Applied Crystallography* 46: 544–549.
- van de Streek, J., and M. A. Neumann. 2014. "Validation of Molecular Crystal Structures from Powder Diffraction Data with Dispersion-Corrected Density Functional Theory (DFT-D)." *Acta Crystallographica Section B: Structural Science, Crystal Engineering and Materials* 70: 1020–1032.
- Von Dreele, R. B. 1997. "Quantitative texture analysis by Rietveld refinement." *Journal of Applied Crystallography* 30: 517–525.
- Wavefunction, Inc. *Spartan '24. V. 1.0.0*. Irvine CA. Wavefunction Inc. 2023.